

Proceeding Paper

Beamforming Techniques for Resilient Navigation with Small Antenna Arrays [†]

Lucía Pallarés-Rodríguez ^{*}, Sergi Locubiche-Serra, Guillem Foreman-Campins, Gonzalo Seco-Granados and José A. López-Salcedo

Department of Telecommunications and Systems Engineering, IEEC-CERES, Universitat Autònoma de Barcelona (UAB), Bellaterra, 08193 Barcelona, Spain; jose.salcedo@uab.cat (J.A.L.-S.)

^{*} Correspondence: lucia.pallares@autonoma.cat

[†] Presented at the European Navigation Conference 2023, Noordwijk, The Netherlands, 31 May–2 June 2023.

Abstract: This paper presents a comparative benchmarking of different beamforming techniques for robust multipath and spoofing mitigation in handheld receivers equipped with a small number of antenna elements. In the field of Global Navigation Satellite Systems (GNSSs), multipath and spoofing have become major sources of signal degradation, whereby the presence of closely spaced replicas of the signal of interest hampers the receiver's performance. Spatial filtering through the use of antenna arrays is one appealing approach to combat these effects. However, the upward trend in device miniaturization poses a serious concern for spatial filtering in handheld devices such as tablets or smartphones, particularly for the case of decimeter-wave signals such as in GNSSs. The terminal size constraints lead to deploying arrays with very few antennas, thus degrading the mitigation performance of the above impairments. This work explores the feasibility of performing robust multipath and spoofing mitigation in GNSS receivers with antenna arrays of very small sizes. Simulation results on four-antenna rectangular and two-antenna linear array distributions are provided, showing that the reduction in array size can be counteracted by the use of advanced beamformers.

Keywords: array processing; beamforming; handheld; multipath mitigation; spatial filtering; spoofing mitigation



Citation: Pallarés-Rodríguez, L.; Locubiche-Serra, S.; Foreman-Campins, G.; Seco-Granados, G.; López-Salcedo, J.A. Beamforming Techniques for Resilient Navigation with Small Antenna Arrays. *Eng. Proc.* **2023**, *54*, 27. <https://doi.org/10.3390/ENC2023-15466>

Academic Editors: Tom Willems and Okko Bleeker

Published: 29 October 2023



Copyright: © 2023 by the authors. Licensee MDPI, Basel, Switzerland. This article is an open access article distributed under the terms and conditions of the Creative Commons Attribution (CC BY) license (<https://creativecommons.org/licenses/by/4.0/>).

1. Introduction

Wireless communications and navigation applications are experiencing a massive proliferation in urban environments thanks to the increasing widespread deployment of enabling technologies such as 5G, the Internet-of-Things (IoT) and Global Navigation Satellite Systems (GNSSs). This has unveiled the need to cope with signal propagation impairments such as interference, multipath and spoofing that are abundant in such urban environments [1,2]. Multipath is certainly a major concern, and it appears whenever the line-of-sight signal (LOSS) of interest is received from multiple paths and different directions of arrival (DoA) due to reflection in nearby objects. The signal replicas exhibit an additional delay and carrier phase offset with respect to the LOSS, thus distorting the latter and hampering the receiver's performance. Of particular concern is the case of coherent multipath, the worst yet most frequent form of multipath in dense urban cities. It appears that the signal reflections are highly correlated to the LOSS due to the fact that they are received very closely spaced in time, coming from reflecting objects very close to the user's receiver. The need to mitigate coherent signal replicas also appears when the receiver is subject to a spoofing attack, a threat of increasing concern in positioning and navigation applications whereby a malevolent party forges the receiver position after gaining illegitimate control over the latter [3].

The use of array-processing techniques, also known as spatial filtering or beamforming, is known to be the most powerful approach to combat the above impairments [4]. The goal

is to steer the array beam toward the LOSS for signal-to-noise ratio (SNR) maximization, and to place nulls at the DoA of the undesired signals. Some examples of conventional beamformers are the phased array, the Capon [5] and the linear minimum mean square error (LMMSE) [6] techniques. However, more advanced beamformers have recently been proposed in the literature, such as the LMMSE–Capon hybrid [7] and the power-based Capon [8] techniques, which have been specially designed to deal with coherent reflections, thus becoming of particular interest for multipath and spoofing mitigation in challenging environments.

An unexplored problem appears, though, when moving to the arena of handheld devices such as tablets or smartphones, which are driven by constraints on miniaturization, low power consumption and low-cost components. The advent of 5G cellular networks has definitely paved the way for the deployment of antenna arrays in such devices as a de-facto standard in the context of multiple-input, multiple-output (MIMO) systems [9–11]. This is motivated by the use of millimeter-wave signals, allowing the implementation of arrays in an area with tiny dimensions. Some examples can be found in [12,13] for 5G applications. However, this is not the case for other technologies such as GNSS, where the terminal dimensions are still and will be, in the long-term, comparable to the signal carrier wavelength. This poses a serious concern for the practical use of spatial filtering in these devices. While extensive research on antenna arrays has been performed for professional GNSS receivers [14,15], where external arrays with many antennas are used, the case of mass-market handheld receivers where just a small number of embedded antennas can be used still remains, to our best knowledge, an open problem.

Hence, the objective of this paper is to explore the feasibility of performing robust multipath and spoofing mitigation in handheld GNSS devices with a small number of antenna elements. Additionally, the paper evaluates the suitability of new beamformers such as the LMMSE–Capon hybrid and the power-based Capon for compensating the limitations and technological challenges posed by such small arrays. To these ends, a benchmarking of the above-mentioned conventional and new beamforming techniques is carried out in two representative scenarios, namely urban and suburban. Two representative antenna array distributions are considered: four-antenna uniform rectangular and two-antenna uniform linear array distributions, henceforth denoted as URA4 and ULA2, respectively.

2. Fundamentals of Array Processing

2.1. Signal Model

Let us consider an array with L antenna elements that perceives the superposition of a LOSS of interest and a set of M undesired replicas. The signal as perceived by the different antenna elements can be arranged into an $L \times 1$ vector $\mathbf{x}(n)$, thus leading to the following complex baseband signal model at the array output,

$$\mathbf{x}(n) = \alpha_0 \mathbf{a}(\theta_0) s(\tau_0, \varphi_0) + \sum_{m=1}^M \alpha_m \mathbf{a}(\theta_m) s(\tau_m, \varphi_m) + \mathbf{e}(n) \quad (1)$$

with $s(\tau, \varphi) \doteq c(n - \tau) e^{j\varphi}$ being the signal bearing the useful information $c(n)$, τ and φ being the propagation delay and carrier phase, and the subscript $_0$ referring to the LOSS. In (1), α is a complex amplitude encompassing information about the signal power, and $\mathbf{e}(n)$ embeds the noise introduced by each antenna channel. The term $\mathbf{a}(\theta) \in \mathbb{C}^{L \times 1}$ is the spatial signature of the signal coming from direction θ as perceived by the different antennas in the array, and it depends on the antenna inter-separation and array distribution. In the remainder of the paper, we will refer to $\mathbf{a}(\theta_0)$ as simply \mathbf{a}_0 .

The samples in (1) collected during an observation interval of N samples can be arranged into the following $L \times N$ matrix

$$\mathbf{X} \doteq [\mathbf{x}(0) \quad \mathbf{x}(1) \quad \dots \quad \mathbf{x}(N-1)] \quad (2)$$

and we also define the following $N \times 1$ signal vector,

$$\mathbf{s}(\tau, \varphi) \doteq [s(-\tau, \varphi) \quad s(1 - \tau, \varphi) \quad \dots \quad s(N - 1 - \tau, \varphi)]^T. \quad (3)$$

The definitions in (2) and (3) will be used later in Section 3 in the description of the beamforming techniques.

2.2. The Beamforming Principle

Beamforming is nothing but the linear combination of the signal samples coming from each of the antennas in the receiver array, with the aim of concentrating the array beam toward a specific DoA and filtering out any other contribution coming from a different DoA. This is performed by applying a set of spatial filtering coefficients or *weights* to the signal in (1) perceived by the array. This is

$$y(n) = \mathbf{w}^H \mathbf{x}(n) \quad (4)$$

where $\mathbf{w} \in \mathbb{C}^{L \times 1}$ is the weight vector, and $y(n)$ is the signal at the beamformer output. Note that $y(n)$ is a scalar magnitude, and it can thus be understood as the output of an equivalent *smart* single antenna. The problem, then, boils down to determining the coefficients in \mathbf{w} that satisfy a given optimization criterion. This is where the beamforming techniques come into play, as explained next.

3. Selected Beamforming Techniques

This section provides a brief description of a set of beamforming techniques that have been selected for their implementation in user terminals with a small number of antennas, and tested later in Section 4. Note that most of them rely on having prior knowledge about the DoA of the LOSS to be spatially filtered. Such knowledge can be obtained by resorting to maximum likelihood estimation [16], spectral estimation methods [17], or, in some applications such as in GNSS, this information can easily be obtained from the satellite ephemeris and the orientation of the user's terminal. In any case, determining the DoA of the LOSS remains out of the scope of the present paper, and it will be assumed to be a priori known henceforth.

3.1. Phased Array

The *phased array* beamformer (PHA), often referred to as *delay-and-sum* (DAS) in the literature, is the most straightforward form of beamforming. The underlying idea is to correct the diverse phase delays at which the signal will arrive at each antenna element. To this end, the weights \mathbf{w}_{PHA} become those that maximize the response of the array at the LOSS DoA, that is, those that maximize the power of the output beamformer $y(n)$. These weights are given by

$$\mathbf{w}_{\text{PHA}} = \frac{1}{L} \mathbf{a}_0 \quad (5)$$

which are nothing but the steering vectors of the impinging LOSS signal. This beamformer can thus be understood as the spatial matched filter to the spatial signature of the received signal when the spatial noise is uncorrelated among antenna elements. However, its simplicity is counteracted by a poor performance when it comes to canceling the signals impinging on the array from particular directions.

3.2. Capon Beamformer

The *Capon* beamformer (CAP), also known as the *minimum variance distortionless response* (MVDR), is the most general beamforming approach. The beauty is that the array beam pattern is controlled by applying a series of constraints to the different directions to be either pointed at or nulled out. More particularly, the underlying idea of the CAP is

to minimize the power at the beamforming output under the constraint that the LOSS be, conversely, unaltered. This is

$$\min_{\mathbf{w}} P_y = \min_{\mathbf{w}} \mathbf{w}^H \mathbf{R}_X \mathbf{w} \text{ subject to } \mathbf{a}_0^H \mathbf{w} = 1 \quad (6)$$

where $\mathbf{R}_X \doteq E[\mathbf{X}\mathbf{X}^H] \in \mathbb{C}^{L \times L}$ is the auto-correlation matrix of the data in \mathbf{X} , and the term $\mathbf{a}_0^H \mathbf{w} = 1$ is the so-called distortionless response constraint. After some mathematical calculations with Lagrange multipliers, the weights \mathbf{w}_{CAP} become [5]

$$\mathbf{w}_{\text{CAP}} = \frac{\mathbf{R}_X^{-1} \mathbf{a}_0}{\mathbf{a}_0^H \mathbf{R}_X^{-1} \mathbf{a}_0}. \quad (7)$$

3.3. Linear Minimum Mean Square Error Beamformer

The *linear minimum mean square error* (LMMSE) beamformer exploits the temporal diversity between the LOSS and the undesired reflections by comparing the received signal with some reference signal generated locally at the receiver. GNSS signals are a clear example of the latter, where such a reference signal is the local code replica used for despreading, that is, $\mathbf{s}(\tau, \varphi)$. The LMMSE beamformer aims at minimizing the MSE of the error between $\mathbf{s}(\tau, \varphi)$ and the array output \mathbf{X} . The solution to this problem is given by [6]

$$\mathbf{w}_{\text{LMMSE}}(\tau_0, \varphi_0) = \mathbf{R}_X^{-1} \mathbf{r}_{X\mathbf{s}}(\tau_0, \varphi_0) \quad (8)$$

with $\mathbf{r}_{X\mathbf{s}}(\tau, \varphi) \doteq E[\mathbf{X}\mathbf{s}^*(\tau, \varphi)] \in \mathbb{C}^{L \times 1}$ being the cross-correlation between the array output and reference signals. The beauty of this approach is that it does not require knowledge on the DoA to be pointed at. On the downside, and as a result of the latter, severe LOSS degradation may be incurred.

3.4. LMMSE–Capon Hybrid Beamformer

The *hybrid beamformer* (HYB) circumvents the limitations of the LMMSE by combining the latter with the CAP exploiting the spatial reference of the LOSS. The beauty of the HYB is that it allows for an iterative implementation by making use of the recursive least squares (RLS) algorithm. It involves a computational load affordable for current microprocessors, thus making the technique suitable for handheld devices. The weights \mathbf{w}_{HYB} are computed as follows [7]:

$$\mathbf{w}_{\text{HYB}}(\tau_0, \varphi_0) = \alpha_0^* \mathbf{w}_{\text{LMMSE}}(\tau_0, \varphi_0) + \beta(\tau_0, \alpha_0) \mathbf{w}_{\text{CAP}} \quad (9)$$

where $\beta(\tau_0, \alpha_0) \doteq 1 - \alpha_0^* \mathbf{a}_0^H \mathbf{w}_{\text{LMMSE}}(\tau_0, \varphi_0)$.

3.5. Power-Based Capon Beamformer

In the presence of replicas that are correlated with the LOSS of interest, matrix \mathbf{R}_X is composed of the LOSS auto-correlation plus some cross-correlation terms between the LOSS and the replicas. As a consequence, the CAP beamformer \mathbf{w}_{CAP} can mix both contributions when minimizing the power at its output, thus eventually leading to an undesired cancellation of the LOSS. In that sense, the *power-based Capon* beamformer (PBC) circumvents this limitation by determining the cross-correlation terms in \mathbf{R}_X and eliminating their effect from the latter prior to applying beamforming onto $\mathbf{x}(n)$.

Briefly, we define $\boldsymbol{\kappa}(\tau_0, \varphi_0) \doteq \alpha_0 \mathbf{r}_{X\mathbf{s}}(\tau_0, \varphi_0) - \alpha_0^2 \mathbf{a}_0$. The cross-correlation terms in \mathbf{R}_X , denoted as $\boldsymbol{\Gamma}_X(\tau_0, \varphi_0) \in \mathbb{C}^{L \times L}$, are as follows [8]:

$$\boldsymbol{\Gamma}_X(\tau_0, \varphi_0) = \mathbf{a}_0 \boldsymbol{\kappa}(\tau_0, \varphi_0)^H + \boldsymbol{\kappa}(\tau_0, \varphi_0) \mathbf{a}_0^H. \quad (10)$$

Then, by defining a new auto-correlation matrix $\tilde{\mathbf{R}}_{\mathbf{X}}(\tau_0, \varphi_0) \doteq \mathbf{R}_{\mathbf{X}} - \mathbf{\Gamma}_{\mathbf{X}}(\tau_0, \varphi_0)$, the PBC beamformer is given by

$$\mathbf{w}_{\text{PBC}}(\tau_0, \varphi_0) = \frac{\tilde{\mathbf{R}}_{\mathbf{X}}^{-1}(\tau_0, \varphi_0) \mathbf{a}_0}{\mathbf{a}_0^H \tilde{\mathbf{R}}_{\mathbf{X}}^{-1}(\tau_0, \varphi_0) \mathbf{a}_0} \quad (11)$$

which is the CAP in (6) after replacing $\mathbf{R}_{\mathbf{X}}$ with $\tilde{\mathbf{R}}_{\mathbf{X}}(\tau_0, \varphi_0)$.

4. Performance Analysis

This section provides the results of the performance assessment for the beamformers described in Section 3 in the context of a handheld device with either two- or four-antenna elements. Without loss of generality, GNSS signals are considered, where the despreading process leads to a correlation peak with time support of $\pm T_c$ around τ_0 , with T_c termed *chip period*. In both urban and suburban scenarios considered herein, the received signal consists of the superposition of a LOSS and an undesired replica (i.e., $M = 1$), with carrier-to-noise ratios (C/N_0) of 44 dB-Hz and 41 dB-Hz, respectively. URA4 and ULA2 antenna distributions are considered, where the antennas are separated half a carrier wavelength apart from one another. The array is assumed to be perfectly calibrated for simplicity, and additive white Gaussian noise (AWGN)-independent antenna channels are adopted. The beamformers are implemented within a closed loop where the determination of τ_0 and φ_0 , denoted as $\hat{\tau}_0$ and $\hat{\varphi}_0$, is carried out through a delay-locked loop (DLL) and a phase-locked loop (PLL), respectively, thus providing estimates in a timely manner and, consequently, allowing for some statistical averaging over time. For the correlation terms $\mathbf{R}_{\mathbf{X}}$ and $\mathbf{r}_{\mathbf{X}s}(\tau_0, \varphi_0)$, we resort to the sample correlations $\hat{\mathbf{R}}_{\mathbf{X}} \doteq \frac{1}{N} \mathbf{X} \mathbf{X}^H$ and $\hat{\mathbf{r}}_{\mathbf{X}s}(\hat{\tau}_0, \hat{\varphi}_0) \doteq \frac{1}{N} \mathbf{X} \mathbf{s}^*(\hat{\tau}_0, \hat{\varphi}_0)$, respectively, with $N = 49$ samples. Two different metrics are employed for the performance analysis. On the one hand, there is the cancellation of the replica, which measures the ratio between the amount of power of the replica canceled out by the beamformers and the LOSS power. On the other hand, there is the well-known *multipath error envelope* (MEE), which measures the errors induced by the computation of $\hat{\tau}_0$ compared to the true value τ_0 . In GNSS, the MEE is directly linked to the error in the estimated receiver position.

4.1. Urban Scenario

Urban scenarios are characterized by the abounding presence of obstacles and tall buildings, thus having sky visibility reduced to a small region in the vertical direction. Hence, the signals are prone to be received from high elevation angles. In that sense, the LOSS and the replica are considered herein to impinge from 80° and 60° elevation, respectively. An azimuth angle of 30° is adopted for both.

Figure 1 illustrates the cancellation of the replica as a function of the delay spacing between the latter and the LOSS, normalized to T_c . Any spacing below one is considered as correlated. The top plot depicts the ULA2 case, and the bottom plot depicts the URA4 case. When it comes to conventional beamformers, the PHA presents very poor mitigation performance, which remains the same irrespective of the replica delay. The CAP is even observed to amplify the undesired replica when highly correlated with the LOSS, in an attempt to level the power of the replica to that of the LOSS. It is not until signals become uncorrelated that the CAP provides acceptable performance, thus making it unsuitable for coherent multipath and spoofing mitigation. The LMMSE seems to provide better performance compared to the PHA and CAP in terms of replica cancellation, but, in contrast, it is found to incur dramatic LOSS degradation, reaching power drops of up to 30 dB. These results apply to both ULA2 and URA4.

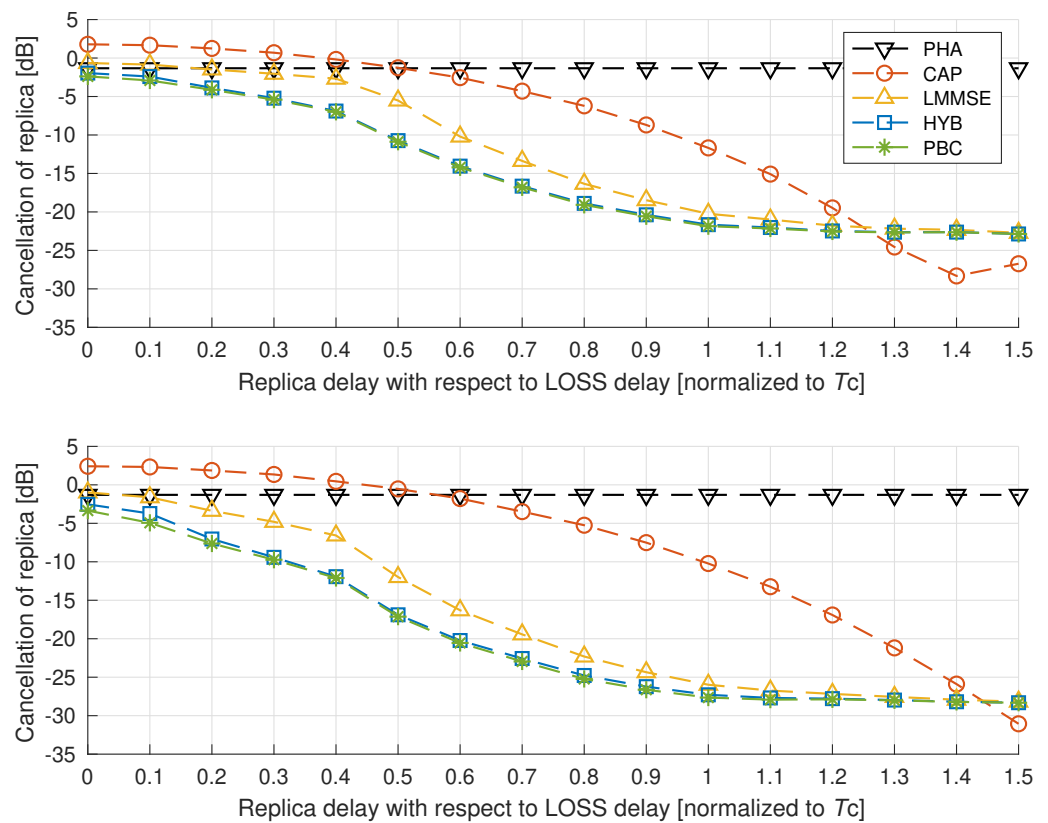


Figure 1. Cancellation of replica with respect to its delay in an urban scenario with ULA2 (top) and URA4 (bottom) array distributions.

Interestingly, the poor performances described above are overcome by the use of more sophisticated beamformers. This is the case for the HYB and PBC. They show the best replica cancellation performance even for highly correlated signals, and it improves rapidly when increasing the replica delay. The latter occurs particularly for the URA4 case, where the cancellation shows a steeper behavior than in ULA2. More specifically, a cancellation of more than 10 dB is achieved in URA4 for as few as 0.3 replica delay, whereas the same performance requires 0.5 replica delay in ULA2, a point where the cancellation in URA4 already exceeds 15 dB. In that sense, it is observed that the gain provided by the use of URA4 with respect to the smaller ULA2 lies in the range of 3–5 dB.

The above observations can also be inferred from the MEE results depicted in Figure 2, which ultimately unveil the impact of mitigation on the receiver performance. The CAP presents a detrimental behavior particularly when signals are highly correlated, with MEE values exceeding 60 m. The PHA provides a slight gain compared to when no beamforming (labeled as “No BF” in the figure) is performed, by decreasing the MEE from 25 m down to 20 m. However, acceptable MEE is not achieved until the signals become uncorrelated. In that sense, conventional beamformers are outperformed by the HYB and PBC, where the MEE barely exceeds 10 m and 5 m for ULA2 and URA4, respectively, and as few as 0.5 replica delay are required for the MEE to drop down below 5 m in both.

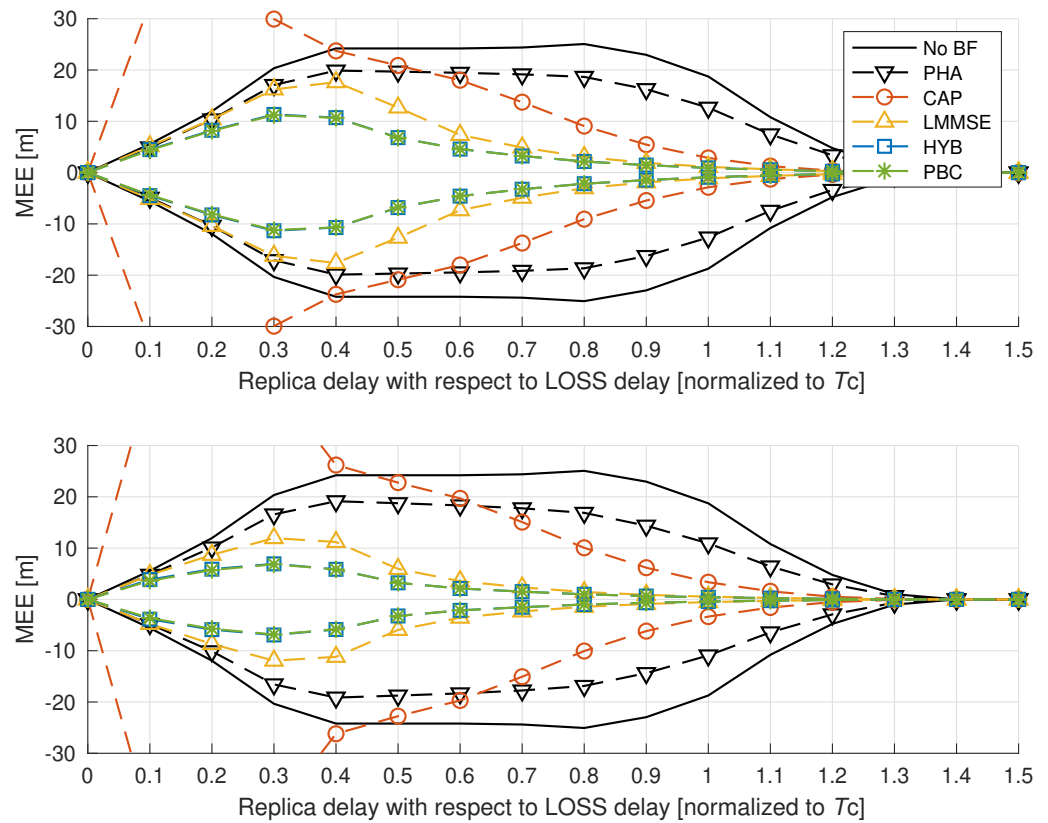


Figure 2. MEE in an urban scenario with ULA2 (top) and URA4 (bottom) array distributions.

4.2. Suburban Scenario

Suburban scenarios comprise those in the city outskirts and residential areas with small buildings, thus having a wider sky visibility than in urban environments. In this case, the LOSS and the replica are considered to impinge from 60° and 20° elevation, respectively. The azimuth angle is also kept here at 30° for both signals.

Figures 3 and 4 depict the replica cancellation and MEE results, respectively, for the suburban scenario. The very same conclusions to those in the urban scenario can be extracted here. Conventional techniques such as the PHA and CAP are outperformed by the HYB and PBC. In terms of replica cancellation, whereas the former two provide practically the same performance as in the urban case, the latter two present a steeper behavior and do provide a gain of ~5 dB along all replica delays. This means that a cancellation of 10 dB is now achieved in ULA2 with as little as 0.3 delay, whereas at this point the cancellation already exceeds 15 dB in URA4. In terms of MEE, conventional beamformers exceed values of 10 m while requiring signals to become separated enough to improve these results. In contrast, the HYB and PBC present MEE no larger than 5 m in ULA2 with only 0.3 replica delay, a point at which the MEE is already below 5 m in URA4. Therefore, the MEE performance in the urban case is even improved in the suburban case by an amount of 3–5 m. These results conclude on the feasibility to perform multipath and spoofing mitigation in ULA2 and URA4 arrays by implementing advanced beamforming techniques such as the HYB and PBC.

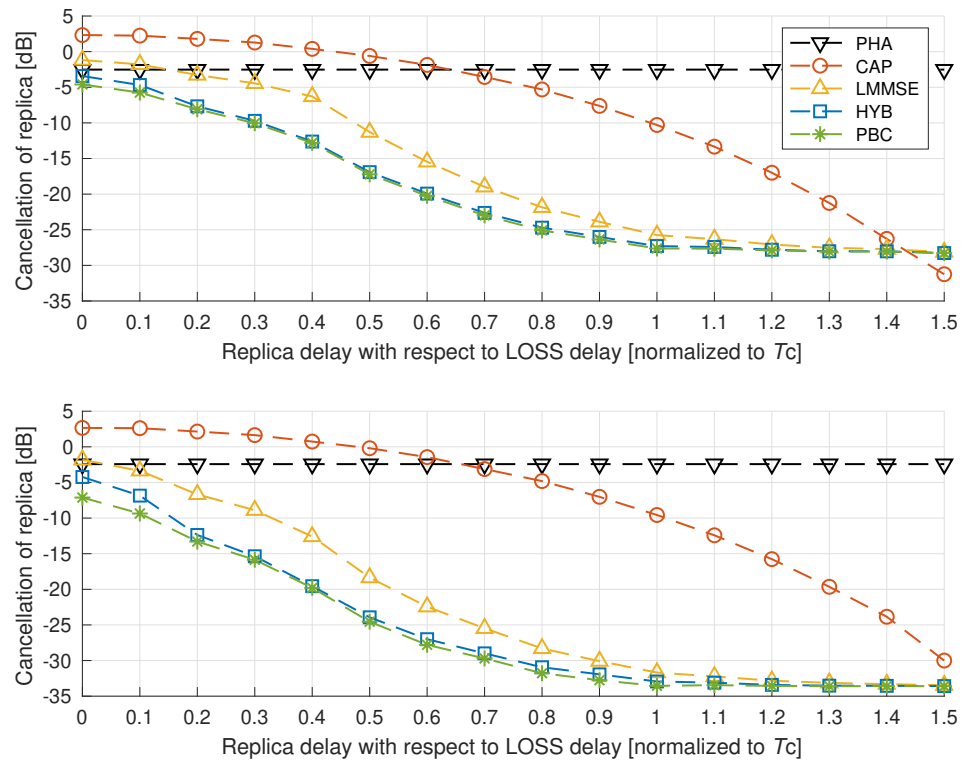


Figure 3. Cancellation of replica with respect to its delay in a suburban scenario with ULA2 (top) and URA4 (bottom) array distributions.

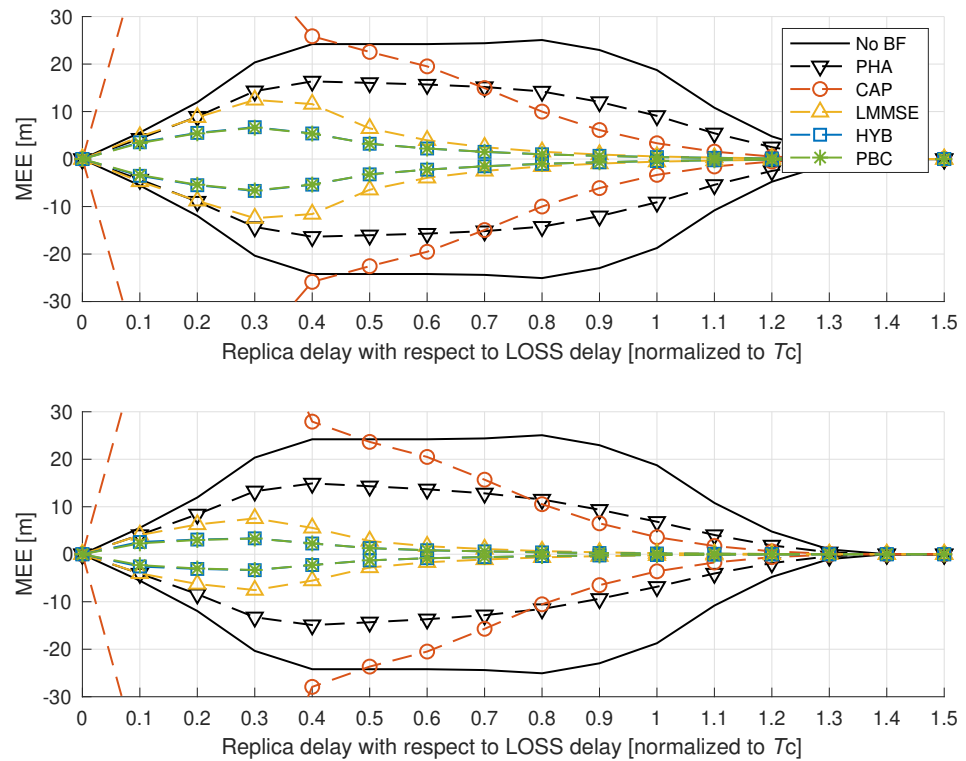


Figure 4. MEE in a suburban scenario with ULA2 (top) and URA4 (bottom) array distributions.

5. Conclusions

In this paper, we have evaluated the feasibility of performing robust multipath and spoofing mitigation with spatial filtering techniques in GNSS antenna arrays of a very small size. In particular, four-antenna rectangular and two-antenna linear arrays have been

considered in a simulation campaign carried out for benchmarking different beamforming techniques in challenging environments, namely urban and suburban. The simulation results have shown the goodness of the LMMSE–Capon hybrid and the power-based Capon beamformers in such small arrays, particularly in the presence of coherent multipath and spoofing. Therefore, they have become potential candidates for signal mitigation purposes in decimeter-wave handheld devices, and their use over conventional beamformers has become mandatory to overcome the limitations of small arrays. Furthermore, although four-antenna arrays do provide better performance, comparable results have been obtained for the case of two-antenna arrays, thus confirming the suitability of the latter for the practical implementation of spatial filtering techniques in smaller devices such as smartphones.

Author Contributions: Conceptualization, S.L.-S. and J.A.L.-S.; methodology, L.P.-R. and S.L.-S.; software, L.P.-R., S.L.-S. and G.F.-C.; validation, L.P.-R., S.L.-S. and G.F.-C.; formal analysis, L.P.-R. and S.L.-S.; investigation, L.P.-R. and S.L.-S.; resources, G.S.-G. and J.A.L.-S.; data curation, L.P.-R. and S.L.-S.; writing—original draft preparation, L.P.-R. and S.L.-S.; writing—review and editing, all authors; visualization, L.P.-R. and S.L.-S.; supervision, S.L.-S. and J.A.L.-S.; project administration, J.A.L.-S.; funding acquisition, G.S.-G. and J.A.L.-S. All authors have read and agreed to the published version of the manuscript.

Funding: This work has been supported in part by the Spanish Agency of Research (AEI) under the Research and Development projects PID2020-118984GB-I00/AEI/10.13039/501100011033 and PDC2021-121362-I00/AEI/10.13039/501100011033.

Institutional Review Board Statement: Not applicable.

Informed Consent Statement: Not applicable.

Data Availability Statement: Data are contained within the article.

Conflicts of Interest: The authors declare no conflict of interest.

References

1. Sahmoudi, M.; Amin, M.G. Optimal Robust Beamforming for Interference and Multipath Mitigation in GNSS Arrays. In Proceedings of the IEEE International Conference on Acoustics, Speech and Signal Processing (ICASSP), Honolulu, HI, USA, 15–20 April 2007; Volume 3, pp. 693–696.
2. Psiaki, M.L.; O’Hanlon, B.W.; Powell, S.P.; Bhatti, J.A.; Wesson, K.D.; Schofield, T.E. GNSS spoofing detection using two-antenna differential carrier phase. In Proceedings of the 27th International Technical Meeting Satellite Division Inst. Navigation (ION GNSS+), Tampa, FL, USA, 8–12 September 2014; pp. 2776–2800.
3. Psiaki, M.L.; Humphreys, T.E. GNSS spoofing and detection. *Proc. IEEE* **2016**, *104*, 1258–1270. [[CrossRef](#)]
4. Swindlehurst, A.L.; Jeffs, B.D.; Seco-Granados, G. Applications of Array Signal Processing. In *Academic Press Library in Signal Processing. Array and Statistical Signal Processing*; Chapter 20; Academic Press: Cambridge, MA, USA, 2014; Volume 3, pp. 859–953.
5. Capon, J. High-resolution frequency-wavenumber spectrum analysis. *Proc. IEEE* **1969**, *57*, 1408–1418. [[CrossRef](#)]
6. Konovaltsev, A.; Antreich, F.; Hornbostel, A. Performance assessment of antenna array algorithms for multipath and interferers mitigation. In Proceedings of the Workshop on GNSS Signals & Signal Processing (GNSS SIGNALS), Noordwijk, The Netherlands, 24–25 April 2007.
7. Seco-Granados, G.; Fernández-Rubio, J.; Fernández-Prades, C. ML estimator and hybrid beamformer for multipath and interference mitigation in GNSS receivers. *IEEE Trans. Signal Process.* **2005**, *53*, 1194–1208. [[CrossRef](#)]
8. Mañosas-Caballú, M.; Swindlehurst, A.L.; Seco-Granados, G. Power-based Capon beamforming: Avoiding the cancellation effects of GNSS multipath. *Signal Process.* **2021**, *180*, 107891. [[CrossRef](#)]
9. Larsson, E.G.; Edfors, O.; Tufvesson, F.; Marzetta, T.L. Massive MIMO for next generation wireless systems. *IEEE Commun. Mag.* **2014**, *52*, 186–195. [[CrossRef](#)]
10. Rusek, F.; Persson, D.; Lau, B.K.; Larsson, E.G.; Marzetta, T.L.; Edfors, O.; Tufvesson, F. Scaling Up MIMO: Opportunities and Challenges with Very Large Arrays. *IEEE Signal Process. Mag.* **2013**, *30*, 40–60. [[CrossRef](#)]
11. Vook, F.W.; Ghosh, A.; Thomas, T.A. MIMO and beamforming solutions for 5G technology. In Proceedings of the IEEE MTT-S International Microwave Symposium (IMS2014), Tampa, FL, USA, 1–6 June 2014; pp. 1–4.
12. Chattha, H.T. 4-Port 2-Element MIMO Antenna for 5G Portable Applications. *IEEE Access* **2019**, *7*, 96516–96520. [[CrossRef](#)]
13. Parchin, N.O.; Al-Yasir, Y.I.A.; Ali, A.H.; Elfergani, I.; Noras, J.M.; Rodriguez, J.; Abd-Alhameed, R.A. Eight-Element Dual-Polarized MIMO Slot Antenna System for 5G Smartphone Applications. *IEEE Access* **2019**, *7*, 15612–15622. [[CrossRef](#)]
14. Vagle, N.; Broumandan, A.; Jafarnia-Jahromi, A.; Lachapelle, G. Performance analysis of GNSS multipath mitigation using antenna arrays. *J. Glob. Position. Syst.* **2016**, *14*, 4. [[CrossRef](#)]

15. Brenneman, M.; Morton, J.; Yang, C.; Van Graas, F. Mitigation of GPS multipath using polarization and spatial diversities. In Proceedings of the International Technical Meeting of the Satellite Division of The Institute of Navigation (ION GNSS 2007), Fort Worth, TX, USA, 25–28 September 2007; pp. 1221–1229.
16. Stoica, P.; Sharman, K.C. Maximum likelihood methods for direction-of-arrival estimation. *IEEE Trans. Acoust. Speech Signal Process.* **1990**, *38*, 1132–1143. [[CrossRef](#)]
17. Roy, R.; Kailath, T. ESPRIT-estimation of signal parameters via rotational invariance techniques. *IEEE Trans. Acoust. Speech Signal Process.* **1989**, *37*, 984–995. [[CrossRef](#)]

Disclaimer/Publisher’s Note: The statements, opinions and data contained in all publications are solely those of the individual author(s) and contributor(s) and not of MDPI and/or the editor(s). MDPI and/or the editor(s) disclaim responsibility for any injury to people or property resulting from any ideas, methods, instructions or products referred to in the content.